Nonlinear response of tropical lower stratospheric temperature and water vapor to ENSO

Chaim I Garfinkel[1], Amit Gordon[1], Luke D Oman[2], Feng Li[3], Sean Davis[4], and Steven Pawson[2]

[1]The Fredy and Nadine Herrmann Institute of Earth Sciences, Hebrew University of Jerusalem, Jerusalem, Israel.
[2] NASA Goddard Space Flight Center, Greenbelt, MD, USA.
[3] Universities Space Research Association, Columbia, MD, USA.
[4] NOAA Earth System Research Laboratory, Boulder, CO, USA.

Correspondence to: Chaim I. Garfinkel (chaim.garfinkel@mail.huji.ac.il)

Abstract. A series of simulations using the NASA Goddard Earth Observing System Chemistry-Climate Model are analyzed in order to assess interannual and sub-decadal variability in tropical lower stratospheric temperature and water vapor over the past 35 years. The impact of El Niño-Southern Oscillation in this region is nonlinear. While moderate El Niño events lead to cooling in this region, strong El Niño events lead to warming, even as the response of the large scale Brewer Dobson Circulation appears to scale nearly linearly with El Niño. This nonlinearity is shown to arise from the response in the Indian Ocean to El Niño: strong El Niño events that lead to warming in the Indian Ocean lead to tropospheric warming extending into the tropical tropopause layer and up to the cold point, where it allows for more water vapor to enter the stratosphere. The net effect is that both strong La Niña and strong El Niño events lead to enhanced entry water vapor and stratospheric moistening. These results lead to the following interpretation of the contribution of sea surface temperatures to the millennial drop in water vapor in late 2000: the very strong El Niño event in 1997/1998 which featured remarkably warm Indian Ocean SSTs, followed by more than two consecutive years of La Niña, led to enhanced lower stratospheric water vapor. As this period ended in early 2001, entry water vapor concentrations declined. This effect led to a decrease in water vapor of 0.14ppmv after 2001, which accounts for approximately 23% of the observed drop.

1 Introduction

The El Niño - Southern Oscillation (ENSO) is the largest source of interannual variability in the Tropics, and manifests as anomalous sea surface temperatures in the Eastern and Central Pacific Ocean. El Niño (EN), the phase with anomalously warm sea surface temperatures in this region, has been shown to impact stratospheric temperatures in both the polar region and in the Tropics (Calvo Fernández et al., 2004; Sassi et al., 2004; Manzini et al., 2006; Garcia-Herrera et al., 2006; Taguchi and Hartmann, 2006; Garfinkel and Hartmann, 2007; Marsh and Garcia, 2007; Free and Seidel, 2009; Calvo et al., 2010). The temperature response in these regions is linked, as ENSO is able to modify the stratospheric mean meridional circulation, also known as the Brewer-Dobson (BD) circulation. During a EN event, anomalous upward propagation and dissipation of planetary waves at middle and high latitudes, and gravity waves and transient synoptic waves in the subtropics

(Garfinkel and Hartmann, 2008; Calvo et al., 2010; Simpson et al., 2011), leads to the acceleration of the BD circulation, resulting in a cooler tropical lower stratosphere and warmer polar stratosphere.

In addition to impacting zonal mean tropical lower stratospheric temperatures, ENSO also impacts the zonal distribution of temperature anomalies. EN leads to a Rossby wave response whereby anomalously warm temperatures are present over the Indo-Pacific warm pool (hereafter warm pool) near the tropopause, with colder temperatures further east over the Central Pacific (Yulaeva and Wallace, 1994; Randel et al., 2000; Zhou et al., 2001; Scherllin-Pirscher et al., 2012). In the tropical tropopause layer water vapor increases in the region with warm anomalies and decreases in the region with cold anomalies, and these local changes in tropical water vapor can exceed 25% below the cold point (Gettelman et al., 2001; Konopka et al., 2016).

The net effect of these temperature anomalies on water vapor above the tropical cold point is complex, as these zonally asymmetric changes are superposed on the larger scale warming or cooling associated with changes of the BDC. The two largest EN events in the satellite era (in 1997/1998 and in 2015/2016) clearly preceded moistening of the tropical lower stratosphere (Fueglistaler and Haynes, 2005; Avery et al., 2017), though the impact of more moderate events is less clear. The net effect of EN in water vapor at the cold point is the residual of the large temperature anomalies in the West Pacific and Central Pacific (Gettelman et al., 2001; Davis et al., 2013; Konopka et al., 2016), and zonally averaged changes in entry water vapor for the moderately-strong ENSO events considered by Gettelman et al. (2001) is 0.1ppmv. In addition, Calvo et al. (2010), Garfinkel et al. (2013a), and Konopka et al. (2016) note the strong seasonal dependence of the effect of EN on stratospheric water vapor: only in spring does EN lead to enhanced water vapor and LN to dehydration, and Garfinkel et al. (2013a) argue that this occurs only as the coldest region near the cold-point tropopause moves closer to India and therefore samples the region which warms moreso than the region which cools.

An additional complexity is the relationship between oceanic temperatures in the Pacific and Indian Ocean during ENSO events. EN leads to warming in the Indian Ocean in the spring following the peak SST anomalies in the Pacific Ocean (Webster et al., 1999; Murtugudde et al., 2000; Su et al., 2001; Schott et al., 2009). However, this relationship between Indian Ocean and Pacific Ocean SSTs is not universal: while the 1997/1998 event was followed by unusually warm Indian Ocean SSTs (Webster et al., 1999; Yu and Rienecker, 2000; Murtugudde et al., 2000), the 1982/1983 event was followed by moderate warming despite comparable strengthed events in the Nino3.4 region of the Pacific Ocean. Teleconnections of EN in spring and summer can be driven both by the Indian Ocean warming and by any lingering SST anomalies in the Pacific. For example, previous work has shown that impacts of EN in parts of East Asia are dominated by the Indian Ocean warming (Xie et al., 2009), while the Arctic stratospheric response to EN is damped by the Indian Ocean warming (Fletcher and Kushner, 2011). It is not clear to what extent the tropical stratospheric response to ENSO, particularly in spring, is governed by these Indian Ocean anomalies and not by any lingering anomalies in the Pacific.

A clearer understanding of the role of ENSO for entry water vapor may be important for understanding the 2000/2001 drop in water vapor (Randel et al., 2004, 2006): Brinkop et al. (2016) argue that the evolution of ENSO from 1997 through 2000 was crucial for this event, such that ENSO variability aliased onto sub-decadal variability. As the amount of water vapor that enters the stratosphere is important for stratospheric chemistry (Solomon et al., 1986) and radiative balance (Forster and Shine, 1999; Solomon et al., 2010), it is important to understand the factors that control its entry into the stratosphere on all timescales.

This paper is motivated by four specific issues related to the lower stratospheric response to ENSO: First, a commonly used method to ascribe stratospheric variability to forcings such as ENSO, the QBO, solar variability, and volcanoes, is to use multiple linear regression (e.g. Crooks and Gray, 2005; Marsh and Garcia, 2007; Mitchell et al., 2015). An assumption underlying this method is that the response to these forcings is linear, i.e. that the response to a given magnitude El Niño is equal and opposite to that of a La Niña event of equal magnitude. Is this assumption really true? Second, Garfinkel et al. (2013a) found that EN events whose sea surface temperature anomalies peak in the Central Pacific (i.e. CP events) lead to dehydration regardless of season while events peaking in the Eastern Pacific (i.e. EP events) lead to spring moistening. However, EP events tend to be stronger than CP events, and it is not clear to what extent the difference found by Garfinkel et al. (2013a) reflects the intensity of the EN event or the flavor of the event. Third, to what extent is the tropical stratospheric response to ENSO governed by SST anomalies in the Indian Ocean sector that typically follow (though with diversity in their amplitude) ENSO? Finally, it has been suggested that SST variability in the Pacific Ocean contributed to the post-2000 drop in water vapor (Rosenlof and Reid, 2008; Garfinkel et al., 2013b) possibly via ENSO (Brinkop et al., 2016), but this contribution has not yet been quantified.

This paper will demonstrate that there are nonlinearities in the lower stratospheric response to ENSO. While typical EN events lead to tropical lower stratospheric cooling and dehydration in winter, the springtime response is nonlinear: strong EN events and LN lead to moistening while weak/moderate EN events lead to dehydration. We clarify that discriminating between CP and EP events may not be crucial, and rather one should discriminate between very strong EN events and moderate EN events. As CP events tend to be weaker than East Pacific events (Johnson, 2013), it is easy to confuse a composite of CP EN events with a composite of moderate EN regardless of type. The source of this nonlinearity is the Indian Ocean response to EN, as Indian Ocean warming leads to moistening of the stratosphere in spring. Finally, we suggest that SST variability in the early 2000s relative to the late 1990s led to 0.14ppmv of dehydration, explaining approximately 23% of the observed drop in water vapor over this period (Randel et al., 2004, 2006).

The data and methods are introduced in Sections 2 and 3. Section 4 demonstrates the nonlinearity of ENSO's effect on tropical lower stratospheric temperature and water vapor. In order to better understand the nonlinearities evident in Section 4, Section 5 considers more closely the strongest EN event covered by our model experiments - the event in the winter of 1997/1998 - and highlights the importance of the Indian Ocean. Section 6 considers implications of the interannual variability for the millennial drop in 2001 and for the EN event in 2015/2016. The supplemental material discusses the linearity of the influence of ENSO on the BDC.

2 Data

We analyze the MERRA (Modern-era retrospective analysis for research and applications; Rienecker et al., 2011) reanalysis, the merged water vapor product from SWOOSH v2.5 (Davis et al., 2016), and output from atmospheric chemistry-climate general circulation models (GCMs) and coupled ocean-atmosphere GCMs on various time scales. The Goddard Earth Observing System Chemistry-Climate Model, Version 2 (GEOSCCM, Rienecker et al, 2008) couples the GEOS-5 (Rienecker et al, 2008;

Molod et al., 2012) atmospheric general circulation model to the comprehensive stratospheric chemistry module StratChem (Pawson et al., 2008). The model has 72 vertical layers, with a model top at 0.01 hPa, and all simulations discussed here were performed at 2° latitude x 2.5° longitude horizontal resolution. The model spontaneously generates a QBO (Molod et al., 2012). The model vertical levels between 140hPa and 50hPa are located at 139.1hPa, 118.3hPa, 100.5hPa, 85.4hPa, 72.6hPa, 61.5hPa, and 52.0hPa; output is plotted at standard pressure levels.

The convection scheme used in GEOSCCM is based on Relaxed Arakawa-Schubert (Moorthi and Suarez, 1992; Rienecker et al, 2008), and the cloud ice parameterization is described in Molod et al. (2012). Note that there is cloud ice in the version of the model under consideration here up to 85hPa (as is evident in our results below). To the extent that entry water vapor is controlled by large scale temperature patterns and the relatively crude ice parameterization in the current generation of the model, we expect that our model captures the response of water vapor to ENSO. That being said, more advanced treatments of ice clouds are currently under development, and hence similar studies must be performed as models improve.

A series of integrations were performed with the GEOSCCM, and they are listed in Table 1 and described below. They fall into two classes: coupled ocean-atmosphere simulations, and historical-SSTs simulations with an atmospheric chemistry-climate general circulation model (AGCM). Both modeling frameworks have their advantages: coupled ocean-atmosphere simulations allow the model to self-consistently develop SST anomalies and teleconnections without violating energetic constraints, and also allow us to examine the stratospheric response to a wider range of ENSO events than have occurred in the historical record. On the other hand, simulations forced with observed SSTs can be more easily compared to the observed response to ENSO.

The model configuration for the coupled ocean-atmosphere simulation is described in Li et al. (2016). The ocean model is the Modular Ocean Model version 5 (Griffies et al., 2015) with 50 vertical layers, and the ocean horizontal resolution is about 1° latitude by 1° longitude. We consider the last 240 years of 340 year-long simulation in which greenhouse gas (GHG) and ozone depleting substance (ODS) forcings are fixed at 1950 levels. Figure 1 compares the 2 meter temperatures over the Nino3.4 region to those over the Indo-Pacific warm pool region in the coupled model and in MERRA reanalysis data. The model simulates stronger ENSO events than have occurred. However, the tendency of EN events to lead to a warmer Indian Ocean is well captured by the model.

The foundation of the AGCM ensemble are the simulations discussed by Garfinkel et al. (2015) and Aquila et al. (2016), though several recent integrations have been added as summarized in Table 1. The simulations form a 42 member ensemble of the period from January 1980 to December 2009, though five integrations have been extended to the near-present to cover the strong EN event in 2015/2016. Such an ensemble is valuable as it frames the forced response to EN common to all integrations within the context of stochastic unforced variability unique to each integration. For 13 integrations, the only time-varying forcings are changing SSTs and sea ice; SSTs and sea ice up to November 2006 are taken from the Met Office Hadley center observational database (Rayner et al., 2006) and from the National Climatic Data Center (Reynolds et al., 2002) since then. For 3 additional integrations, GHG concentrations are from observations up to 2005 and from the Representative Concentrations Pathway 4.5 after 2005 (Meinshausen et al., 2011) in addition to time varying SSTs and sea ice. For 19 additional integrations ODS also vary as observed. For seven additional integrations these forcings plus volcanic eruptions are included (Aquila et al.,

2016); for these seven integrations we discard the winter seasons 1991/1992 and 1992/1993 and the years 1991, 1992, and 1993 from consideration, as the eruption of Mt. Pinatubo had a large impact on the BDC and tropical temperatures in our simulations (Aquila et al., 2016; Garfinkel et al., 2017), and appears to have led to moistening in observational data as well (Fueglistaler, 2012; Dessler et al., 2014). In 1994 the difference in entry water vapor between these seven integrations and the other integrations is less than 0.05ppmv (not shown). Four of these seven integrations also include time varying solar forcing. All simulations considered are summarized in Table 1. These simulations have been performed for various purposes and differ in the forcings included and in the physical parameterizations, but they all include changing SSTs and sea-ice.

GEOSCCM model output is compared to temperatures from MERRA and water vapor from SWOOSH v2.5. Temperatures from MERRA are interpolated to the same 2° latitude x 2.5° longitude degree grid used for the GEOSCCM simulations. In order to isolate the interannual variability, we detrend timeseries for the AGCM simulations and for reanalysis/observations.

Anomalies are computed as follows. A monthly climatology over the full duration of each model experiment, reanalysis product, and observational dataset is computed, and is then subtracted from the raw fields to generate monthly anomalies. The model climatology is computed separately for each model simulation due to differences in the forcing agents and model components used.

Model output necessary to run a Lagrangian trajectory model for these simulations was not archived, and hence we cannot quantify the specific location of dehydration. More generally, the advantage in studying historical changes in water vapor and temperature in free running climate simulations is *not* to form a best estimate of the actual interannual variability; for that purpose, nudged experiments and/or Lagrangian trajectory modeling are far better. Rather, the motivation is four-fold: one, future projections of the temperature and water vapor changes in this region can only be produced by free running climate simulations, and these projections are of limited value if a model's simulation of the past is inconsistent with observational constraints; two, assuming the model is capable of capturing interannual variability, the causes of trends or discontinuities (such as the millennial drop) can be better understood in a framework in which there is no possibility that changes in the observing or modeling system could have led to these trends or discontinuities; three, large ensembles of a free running model can be produced in order to better isolate the forced response from a single EN event from unrelated internal atmospheric variability not forced by anomalies at the ocean surface; fourth, and relatedly, the observational record is not long enough in order to confidently conclude whether the response to ENSO is nonlinear or to confidently separate the impacts of Indian Ocean SSTs from Pacific SSTs due to their strong covariability, and thus only by considering large model ensembles can these effects be confidently identified.

3 Methods

ENSO events are categorized into four groups similar to Hurwitz et al. (2014): Eastern Pacific (EP) EN, characterized by positive sea surface temperature (SST) anomalies in the Nino-3 region (5S - 5N, 210E-270E), and Central Pacific (CP) EN, characterized by positive SST anomalies in the Nino-4 region (5S-5N, 160E-210E), as well as EP and CP La Niña events, characterized by negative SST anomalies in the same two regions. ENSO events are identified based on NDJF seasonal mean

SST anomalies in the ERSSTv4 dataset (Huang et al., 2015) with a 1981-2010 base period, and the same definition is applied to the coupled ocean-atmosphere simulations. EN and LN events are identified when SST anomalies in the Nino3.4 region exceed 0.5K and -0.5K respectively. EN and LN events are further categorized as follows: EP El Niño events are identified when the Nino-3 anomaly is 0.1 K larger than the corresponding Nino-4 anomaly. Similarly, EP La Niña events are identified when the Nino3 anomaly is 0.1 K less than the Nino-4 anomaly. CP El Niño and CP La Niña events are identified analogously. All remaining years, either because they are neutral ENSO or because the Nino-3 and Nino-4 anomalies are within 0.1K, are categorized as "other events". The years included in each composite are listed in Table 2.

Most ENSO events peak in the late fall or early winter, and decay by the following spring. Hence, we focus on the response of the lower stratosphere during the period from November through June.

As discussed in the introduction, it is well known that EN forces an intensified BDC. Hence, in considering the response to ENSO, we consider the response without regressing out the influence of the BDC, as regressing out the BDC misrepresents the net impact of ENSO on the lower stratosphere. We have analyzed the water vapor response upon regressing out the influence of the BDC, and the moistening of the stratosphere during El Niño is more pronounced as expected. We consider two alternate diagnostics of the BDC: the tropical diabatic heating rate and the mean age; the main text shows results for tropical diabatic heating rate, and the supplemental material shows mean age. Details of the mean age calculation can be found in Garfinkel et al. (2017).

A QBO is spontaneously generated in all simulations considered here. The QBO phase differs among these experiments (i.e. the phase does not match observations), and hence many of the complications that arise due to the QBO (e.g. Liang et al., 2011) are not relevant. We have confirmed that regressing out the influence of the QBO at 50hPa has little impact on our model results. However, we linearly regress out variability associated with the zonal wind at 50hPa two months prior for figures that compare model output to observations/reanalysis.

Due to the very slow vertical motions in tropical tropopause layer and relatively faster horizontal motions, entry water vapor is sensitive to the coldest regions in the tropics and not just zonal mean temperatures (i.e. the cold point, Mote et al., 1996; Fueglistaler et al., 2004; Fueglistaler and Haynes, 2005; Oman et al., 2008). We therefore include isotherms corresponding to the coldest region in the tropics on figures of temperature at 100hpa. The climatological cold point is enclosed with a green contour, and the corresponding contour during EN is enclosed in magenta. Temperature anomalies at 85hPa resemble quantitatively those at 100hPa, and we therefore show 100hPa anomalies only for brevity.

The adjusted R^2 (eq 3.30 of Chatterjee and Hadi, 2012) is used to quantify the added value in using a polynomial best fit (e.g. $H_20 \sim a * EN^2 + b * EN$) instead of a linear best-fit (e.g. $H_20 \sim c * EN$) . The adjusted R^2 takes into account the likelihood that a polynomial predictor will reduce the residuals by unphysically over-fitting the data. While in principle the polynomial fit could be preferred if the adjusted-R^2 for the polynomial fit is larger by any amount as compared to the linear R^2, we elect to be conservative and demand that the adjusted R-squared for a polynomial fit exceed the R^2 for a linear fit by 33%. Note that the 33% criteria is subjectively chosen, though results are similar for a slightly modified criteria.

4 Linearity of the ENSO effect in the tropical lower stratosphere

We now consider the seasonality and linearity of the ENSO effect in the tropical lower stratosphere. Figure 2 shows the response of temperature, water vapor, and the BDC to ENSO in the coupled ocean-atmosphere run, from the late fall through late spring. Figure 3 is comparable but for the AGCM integrations, and Figure 4 is comparable but for MERRA and SWOOSH data. The slope and uncertainty of the linear least-squares best fit is indicated on each panel for integrations where a linear best-fit is deemed satisfactory (see the methods section), while the adjusted R^2 is indicated when a parabolic fit is preferred. Different colors are used to distinguish CP from EP events.

We begin with temperature changes in winter. EN leads to strong cooling of the tropical lower stratosphere in winter (Figure 2ad, 3ad), while LN leads to warming relative to the climatology. This temperature response is consistent, to zeroeth order, with the changes in the BDC associated with ENSO: EN leads to an accelerated BDC while LN leads to a decelerated BDC (Figure 2cf and 3cf; see also the supplemental material). In winter, the relationship between ENSO and lower stratospheric conditions are linear; that is, the impact of EN and LN events of similar strength is equal and opposite. The magnitude of these effects, as quantified by the best-fit line, appears to be slightly weaker in the AGCM ensemble as compared to the coupled ocean-atmosphere runs, and this could be because of the difference in the nature of ENSO events or decadal variability.

Figures 2be and 3be considers changes in water vapor in winter. In both the AGCM and the coupled ocean-atmosphere simulations EN leads to dehydration in winter. Even if we linearly regress out the BDC the slope in Jan/Feb is still suggestive of EN leading to dehydration, though the slope is no longer significantly different from zero (not shown). That EN leads to dehydration in winter is in agreement with Calvo et al. (2010), Garfinkel et al. (2013a), and Konopka et al. (2016), who all note the strong seasonal dependence of the effect of EN on stratospheric water vapor.

While the relationship between ENSO and lower stratospheric conditions is linear in winter, it is nonlinear for both water vapor and temperature in spring (bottom two rows of Figure 2 and 3). Namely, a parabolic (e.g. $H_20 \sim a * EN^2$) fit better describes the springtime relationship between ENSO and water vapor and between ENSO and lower stratospheric temperature than a linear fit (Figure 2ghjk and 3ghjk). Hence, strong EN events lead to less cooling than what might have been expected given a linear best-fit, and consistent with this, the strongest EN events lead to more moistening that might have been expected based on a linear best-fit line. This is especially evident in figure 2hk, where the strongest EN events lead to springtime moistening. The AGCM runs capture this effect as well, as the 97/98 EN also leads to moistening (the most extreme EN event in figure 3hk). This effect is explored further in section 5, where we compare the temperature response to the 97/98 EN to other EN events.

It does not matter whether the ENSO event is categorized as a CP or EP event, as the red, black, and blue dots all indicate the same relationship between ENSO and water vapor. However, the strongest EN events tend to be EP in both nature and in the coupled ocean integrations, and hence the nonlinearity is less detectable for CP events. This difference in strength also explains why the compositing approach of Garfinkel et al. (2013a) to characterizing the impact of EP events and CP events can mislead: the atmospheric response to a composite of EP events may differ from the response to a composite of CP events because the events included in the EP composite are stronger, not because of the specific pattern of the SST anomalies.

Finally, it is important to note that for all panels in Figure 2 and 3, the model simulated evolution falls within the observational constraints (Figure 4). Furthermore, the qualitatively different behavior for the 1997/1998 event is evident both for the model experiments and observations. Hence the model reasonably simulates nature. However, the relatively short data record limits the confidence with which we can identify nonlinearities in observational/reanalysis data, and none of the linear best-fit slope estimates for SWOOSH water vapor are statistically significant in either winter or spring.

5 Composite analysis of the 97/98 event as compared to other events

In order to better understand why strong EN events may affect the spring tropical lower stratosphere differently from weak events, we compare the 97/98 event to other EN events in the AGCM GEOSCCM runs. The time evolution of the water vapor anomalies associated with the 97/98 event are shown in Figure 5a, and Figure 5b shows the water vapor anomalies associated with all other EN events. There is clearly a large difference, with the 97/98 event leading to robust moistening peaking at 0.4ppmv in late spring while all other events have little effect.

Figure 6 and 7 show a map view of changes in temperature at 100hPa for the 97/98 event and for all other EP EN events. While in all cases there is relative cooling in the Central Pacific and relative warming over the Warm Pool region (consistent with Yulaeva and Wallace, 1994; Randel et al., 2000; Scherllin-Pirscher et al., 2012), there are clear differences in the temperature pattern of importance for water vapor. In the 97/98 event in winter, the zero-line of temperature anomalies is 30° further east than for the other EP EN events. This zonal shift is of crucial importance for the cold point region, as the coldest region shifts east without shrinking for typical EP EN events (compare the magenta and green isotherms in Figure 7ab) but warms for the 1997/1998 event (i.e. the magenta isotherms in Figure 6 denote a warmer temperature than the green isotherms due to warming of the cold point). The eastward shift in Figure 6b and 7ab and is consistent with the shift in the Lagrangian cold point evident in figure 8 of Hasebe and Noguchi (2016). In spring, there is broad-scale warming over most of the equatorial band for the 97/98 event, while the temperature anomalies are similar to those in winter for moderate EN events (Figure 6cd and 7cd). A similar effect is seen in the MERRA reanalysis (not shown). The net effect is that in winter and especially spring, the 97/98 event led to warming of the cold point and moistening of the stratosphere relative to other EP EN events.

The changes in tropical temperature in GEOSCCM for the 97/98 event and for other events are summarized in Figure 8, which shows the temperature averaged from 5S to 5N from 300hpa to 50hPa. The overall quadrupole structure is similar to that in Liang et al. (2011) and Garfinkel et al. (2013b), and there is an eastward shift of the cold point region. The model captures the warming pattern in reanalysis (compare Figure 8 and S1). Most pertinently, there are clear differences between the changes in 97/98 and those in other EN years: the tropospheric warming is more pronounced and widespread in 97/98 from late winter through to late spring. The net effect is that the cold point region warms in 97/98 but not in the other EN years.

It is important to emphasize that this nonlinearity in the temperature and water vapor response appears to originate from the troposphere. The changes in the BDC appear to be mostly linear in Figures 2, 3, and 4. The wave-driving of the BDC is not the source of the nonlinearity (see the supplemental material). Rather, the 1997/1998 event led to exceptional warming throughout

the tropopause transition layer and at the cold point as is evident in Figures 8 and S1, and hence led to enhanced water vapor entering the stratosphere.

Why was the 97/98 El Niño tropospheric warming so distinct from other events? While this was the strongest El Niño over the period considered by this paper, the 1982/1983 El Niño was not much weaker than the 1997/1998 event as measured by the Nino3.4 index, yet the impact of the 1982/1983 on water vapor was qualitatively different. Furthermore, the upper tropospheric warming in the Central and East Pacific sectors for the 1982/1983 and 1997/1998 events (Figure 8) are similar. This suggests that the Central and East Pacific responses cannot explain the difference in stratospheric response. In contrast, these two events differed quite dramatically in the Indian Ocean (and more generally in zonally averaged tropical temperature). The 1997/1998 event led to remarkable impacts in the Indian Ocean: warm anomalies exceeded 2C locally over the West Indian Ocean and enhanced convection over Africa was anomalously strong even for EN (Webster et al., 1999; Su et al., 2001). Sea surface temperatures north of the equator were anomalously warm in the spring and summer of 1998 as well (Yu and Rienecker, 2000). As discussed in Garfinkel et al. (2013a), the cold point moves toward India in spring and thus warming in this area can impact water vapor. This difference in near surface conditions in the Indo-Pacific and Nino3.4 region is quantified in Figure 1. Conditions during the 1982/1983 event are shown with a red diamond, and during the 1997/1998 event with a large red x. Despite largely similar anomalies in the Nino3.4 region, the 1997/1998 event was characterized by remarkably warm anomalies in the Indo-Pacific that lie in the tail of the warming generated spontaneously in the coupled ocean-atmosphere model.

The importance of Indian Ocean SSTs for entry water vapor is quantified in Figure 9, which shows the regression coefficient between 85hPa water vapor and 2meter temperatures from 5S to 5N at each longitude grid point. We show both the regression coefficient in the annual average with no lag between water vapor and surface temperature and in springtime with 2meter temperatures leading water vapor by two months (Garfinkel et al., 2013a). The black curve shows the regression after linearly regressing out the BDC from the water vapor, and the blue curve regression after linearly regressing out the QBO from the water vapor.

In the annual average, warmer near-surface temperatures over the Central and Eastern Pacific lead to dehydration of the stratosphere in all three data sources, though during spring warming in the eastern Pacific leads to moistening of the stratosphere two months later. More importantly however, stratospheric water vapor is most sensitive to variability in the Indian Ocean basins and the Warm Pool region, with warmer temperatures in this region leading to enhanced water vapor in all three data sources in spring (and if the BDC influence on water vapor is regressed out, also in the annual average). Results are similar if correlations are examined (not shown).

Figure 10 demonstrates that the nonlinearity of the spring stratospheric response to EN is due to Indo-Pacific surface temperatures. It is constructed similarly to Figure 2, but years are stratified by 2meter temperatures from 50E to 150E instead of by the Nino3.4 index. Instead of the pronounced springtime nonlinearity evident in Figure 2, the lower stratospheric response to Indo-Pacific surface temperature is linear in all seasons. In winter, a warmer near surface leads to impacts similar to that of ENSO (compare top row of Figure 2 to 10). In March and April, on the other hand, a warmer Indo-Pacific leads to an accelerated BDC and a colder lower stratosphere, but to no robust changes in water vapor. In May and June, a warmer Indo-Pacific still leads to an accelerated BDC, but despite this accelerated BDC the lower stratosphere moistens. Results are similar for

the AMIP integrations (not shown), with the 1997/1998 event leading to lower stratosphere moistening despite an accelerated BDC.

In summary, an ENSO event that more efficiently warms the mid-troposphere (such as the 1997/1998 event) by modifying SSTs in the Indian Ocean can more efficiently moisten the stratosphere. Strong EN events tend to have a stronger impact on the Indian Ocean than more moderate events (cf. Figure 1), and this tendency accounts for the nonlinearity in the impact of EN on the spring tropical lower stratosphere.

6 Implications for the post-2000 drop and the 2015/2016 EN event

It has been suggested that SST changes in the Indo-Pacific contributed to some of the post-2000 drop in water vapor (Rosenlof and Reid, 2008; Garfinkel et al., 2013b) via ENSO (Brinkop et al., 2016), and here we consider whether the AGCM simulations simulate a drop. Before proceeding, it is important to mention that the 1997/1998 El Niño was followed by nearly three consecutive years of strong La Niña conditions: the Nino3.4 index in the ERSST4 dataset did not drop below -0.5K until March 2001. As discussed above, strong La Niña events also lead to moistening of the stratosphere. The net effect is that ENSO was in a phase that leads to enhanced water vapor during 1998, 1999, and 2000. It has already been documented that QBO and BDC variability are key ingredients for the observed drop (Randel et al., 2006; Fueglistaler, 2012; Fueglistaler et al., 2014; Dessler et al., 2014). Note that the QBO phase in these GEOSCCM experiments does not match that observed, and the specific wave events that drove the accelerated BDC in late 2000 are not nudged to occur in these free-running GEOSCCM simulations either. Hence we do not expect to be able to capture the full magnitude of the drop. However these experiments can be used to quantify the contribution of SSTs to the observed drop, and with these caveats duly noted we now proceed.

Figure 11a shows the evolution of anomalous annual averaged entry water vapor between 5S-5N in the AGCM simulations (excluding the simulations that represent the eruption of Mt. Pinatubo), with the brown line showing the mean across all simulations, the black line showing the mean of the five simulations that have been extended through the end of 2016, and thin lines showing the evolution in those five simulations individually. It is evident from the brown line in Figure 11a that these integrations capture the observed pronounced decrease in the early 2000s. If we define the drop as the difference in water vapor between 2002 through 2004 and 1998 through 2000, the mean magnitude of this dehydration among all integrations is 0.14ppmv, and the maximum drop in any of the integrations is 0.32ppmv. Note that we focus on annual averaged entry water vapor, and so the timing of the drop (between 2000 and 2001) is fully consistent with the timing of the observed drop as calculated by Fueglistaler (2012) and Hasebe and Noguchi (2016). The mean value is approximately 23% of the total drop (which equals 0.62ppmv in the deep tropics if we apply the same definition to SWOOSH data, though as shown by Fueglistaler et al. (2013) the different satellite products that underly the SWOOSH data disagree as to the magnitude of the drop.) As discussed above, the rest of the drop is associated with BDC and QBO variability which these GEOSCCM simulations are not expected to capture. Hence, SST changes contributed to the drop (in agreement with Rosenlof and Reid, 2008), but were not the major forcing factor, consistent with Garfinkel et al. (2013b) and Brinkop et al. (2016). The magnitude of the drop is 0.09ppmv if we consider water vapor area weighted from 60S to 60N.

Finally, five of the integrations have been extended to the near present and hence include the 2015/2016 El Niño event. This event was comparable in strength in the Nino3.4 region to that in 1997/1998, and while it satisfies the criteria we adopt for an EP event, it was less strongly eastern Pacific-focused as compared to the 1997/1998 event. We now consider the evolution of water vapor in those integrations in Figure 11. Note that these simulations are forced with time varying SSTs and sea ice only.

The model simulates a 0.5ppmv increase in H2O in 2016 (annual average) as compared to 2015, approximately 70% of the observed increase. Note that part of the observed increase was due to the phase of the QBO, and the QBO phase in GEOSCCM does not match that in nature. Hence, the model is clearly capable of capturing the enhanced stratospheric water vapor following strong EN events. The seasonal evolution of the change is shown in Figure 5c, and the increase in water vapor occurs in the spring after the EN event has already begun to decay. The moistening in 2016 is comparable to that in 1998 (cf. figure 5ac). Avery et al. (2017) find enhanced cloud ice associated with this event in Calipso data, and we therefore consider whether the model can capture this effect in Figure 11b, which shows tropical cloud ice between 5S-5N at 100hPa. These integrations all simulate a jump in tropical cloud ice at 100hPa of around 0.5ppmv associated with this event, in agreement with Calipso data (Avery et al., 2017), and even at 85hPa cloud ice increases by 0.05ppmv. The spatial distribution of the change in cloud ice at 85hPa in December 2015 is shown in Figure 11c; the pattern of anomalous ice matches that found in Calipso data (see Figure 1 of Avery et al., 2017). Note that these integrations also simulate a drop after 2011 (Urban et al., 2014; Gilford et al., 2016), suggesting that part of this drop was forced by SSTs as well. Hence, in summary, strong EN events lead to an enhanced water vapor response in both GEOSCCM and in nature.

7 Conclusions

Tropical lower stratospheric temperature and water vapor changes have important implications for both stratospheric and tropospheric climate as well as stratospheric ozone chemistry (SPARC-CCMVal, 2010; World Meteorological Organization, 2011, 2014). Hence, it is crucial to understand interannual changes in this region in order to correctly interpret future changes. Analysis of a series of chemistry-climate atmospheric model in two distinct configurations - coupled to an interactive ocean model and forced by historical sea surface temperatures - yielded the following conclusions:

1. The impact of El Niño-Southern Oscillation in this region is nonlinear in spring. While moderate El Niño events lead to cooling in this region, strong El Niño events lead to warming, even as the response of the large scale Brewer Dobson Circulation appears to scale nearly linearly with El Niño. The tropospheric warming associated with strong El Niño events extends into the tropical tropopause layer and up to the cold point, where it allows for more water vapor to enter the stratosphere. The net effect is that both strong La Niña and strong El Niño events lead to enhanced entry water vapor and stratospheric moistening in spring. Only in midwinter is the response linear. The source of the springtime nonlinearity is the Indian Ocean response to El Niño: strong El Niño events lead to a warmer Indian Ocean in spring that then leads to warming and moistening of the tropical lower stratosphere

2. There is no appreciable difference in the tropical lower stratospheric response to Central Pacific versus Eastern Pacific El Niño events, if one controls for the amplitude of the El Niño event. As Eastern Pacific El Niño events tend to be stronger, however, the nonlinear effects discussed above are pronounced mainly for events of this type.

3. The very strong El Niño event in 1997/1998 followed by more than two consecutive years of La Niña led to enhanced lower stratospheric water vapor. As this period ended in early 2001, entry water vapor concentrations declined. The magnitude of this effect is 0.14ppmv, which accounts for approximately 23% of the observed water vapor drop. Hence, it is important to consider SST variability when considering decadal variability in the lower stratosphere, though other forcings were more important for the millenium drop.

In light of these results, we wish to emphasize that two commonly used methodologies in stratospheric research can lead to misleading conclusions. First, multiple linear regression approaches to attributing stratospheric variability in water vapor and temperature to forcings such as ENSO are problematic, as the stratospheric response to ENSO is nonlinear in the tropical lower stratosphere. Second, compositing approaches of ENSO into Central Pacific and Eastern Pacific types can also lead one astray, as Central Pacific El Niños are weaker and a naive compositing analysis cannot distinguish whether a difference in response is due to differences in spatial patterns rather than differences in event amplitude. Specifically, Garfinkel et al. (2013a) compared EP EN events including 1997/1998 to all CP EN events. A more meaningful comparison is EP EN events excluding 1997/1998 to all CP EN events, and our GEOSCCM experiments suggest that there is no difference in stratospheric response for such a comparison of composites.

This study leaves several unanswered questions. First, model output necessary to run a Lagrangian trajectory model for these simulations was not archived, and hence we cannot directly address whether EN modifies the residence time in the coldest regions of the tropical tropopause layer, an effect that was found to be important by Bonazzola and Haynes (2004). However these sampling effects are included implicitly in GEOSCCM, and some of the diversity in response among the 42 ensemble members to an identical SST forcing is almost certainly due to such sampling effects.. Second, and relatedly, it is not clear mechanistically how upper tropospheric warming over the Indian Ocean leads to moistening of the stratosphere. However this effect appears to be consistent with recent suggestions that mid-tropospheric warming can directly lead to a warmer cold point tropopause and wetter stratosphere (Dessler et al., 2013, 2014). Finally, entry water vapor may be influenced by physical processes that are missing or poorly-represented by the current generation of climate models, and hence similar studies must be performed as models improve. However, the nonlinearity of the lower stratospheric response to El Niño is robust in models and is evident in observations, and hence caution must be exercised when deciding on a methodology for analyzing the tropical stratospheric response to El Niño.

Table 1: GEOSCCM Model Experiments

ocean	forcings	integration length	reference
coupled ocean	1950 timeslice	340 (240)	Li et al. (2016)
historical SSTs	SST+sea ice	13x(1980-2009)	5 from Garfinkel et al. (2015), Aquila et al. (2016) + 5 new
historical SSTs	SST+sea ice GHG	3x(1980-2009)	Aquila et al. (2016)
historical SSTs	SST+sea ice+GHG+ODS	19x(1980-2009)	Aquila et al. (2016), Garfinkel et al. (2015)+6 new
historical SSTs	SST+sea ice+GHG+ODS+volcanoes	3x(1980-2009)	Aquila et al. (2016)
historical SSTs	SST+sea ice+GHG+ODS+volcanoes+solar	4x(1980-2009)	Aquila et al. (2016) + CCMI

Table 2: Events composited for AGCM and observations

composite	years
EP El Niño	1982/1983, 1986/1987, 1991/1992, 1997/1998, 2015/2016
CP El Niño	1994/1995 and 2004/2005
EP La Niña	1984/1985, 1995/1996, 1999/2000, 2005/2006, 2007/2008
CP La Niña	1983/1984, 1998/1999, 2000/2001, 2008/2009

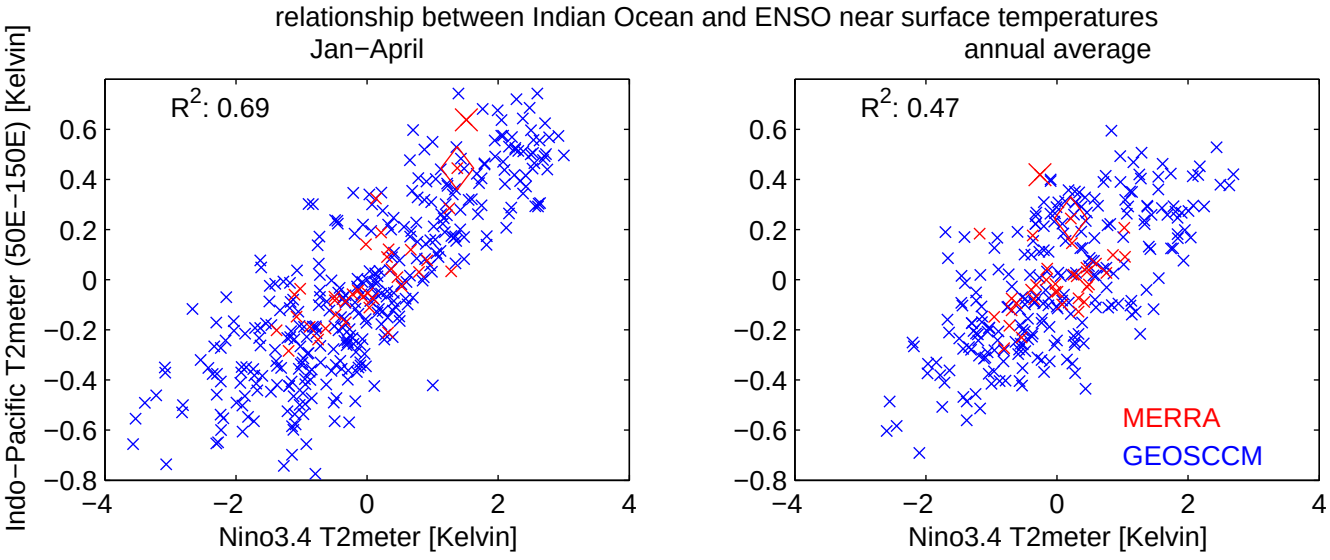

Figure 1. Relationship between near surface temperatures over the Nino3.4 region and over the Indian Ocean and Warm pool region from 5S to 5N in (blue) the GEOSCCM coupled ocean-atmosphere integration and in (red) MERRA reanalysis data. The EN event 1982/1983 is indicated with a large red diamond, and the EN event in 1997/1998 is indicated with a large x. (left) January through April; (right) annual average.

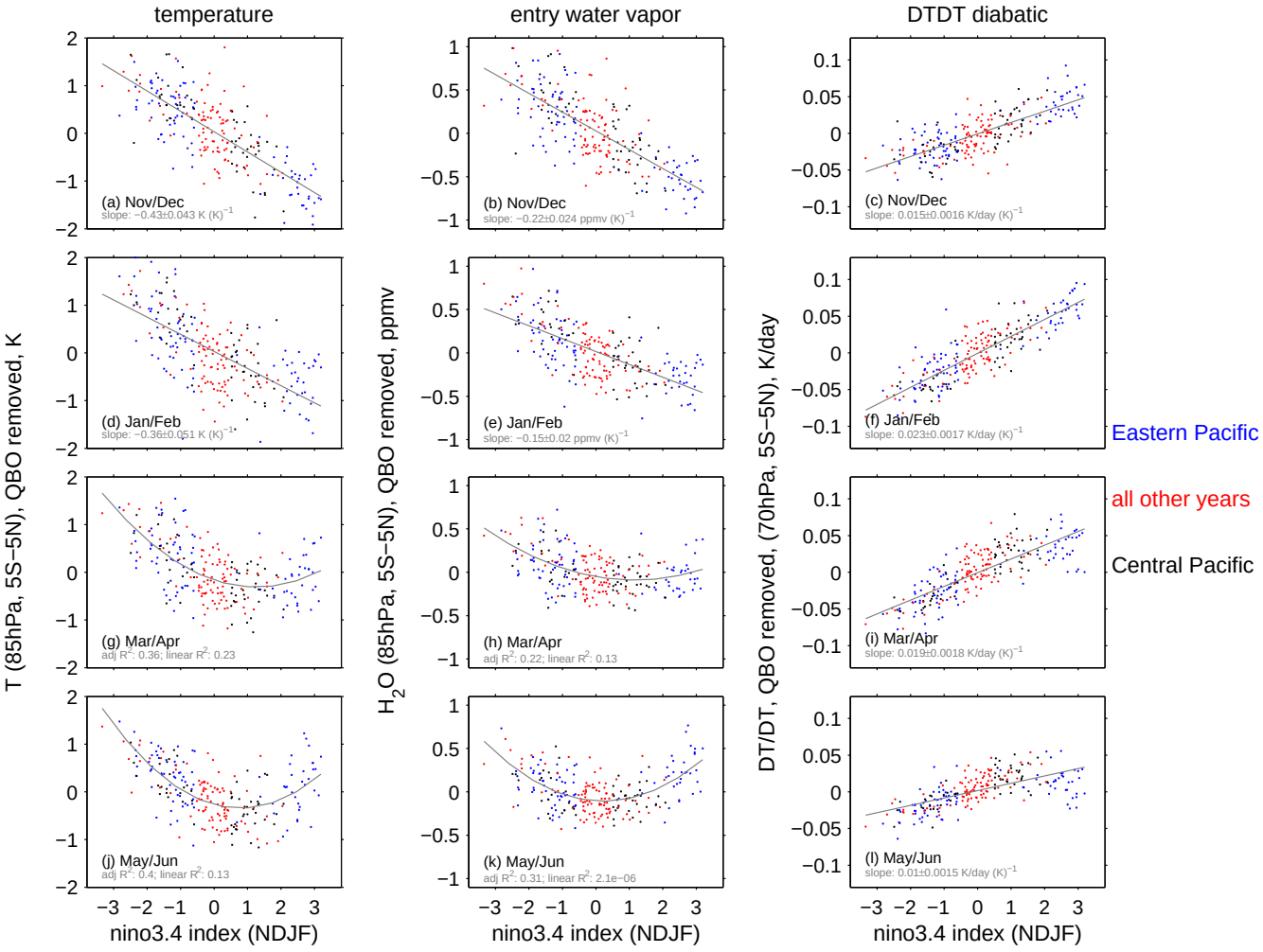

Figure 2. Seasonally resolved anomalies in the tropical lower stratosphere stratified by the Nino3.4 index in NDJF in the coupled ocean-atmosphere GEOSCCM integration. (a-c) November and December; (d-f) January and February; (g-i) March and April; (j-l) May and June. (left) temperature at 85hPa, 5S-5N; (center) water vapor at 85hPa, 5S-5N; (right) diabatic heating rate at 70hPa, 5S-5N. For all quantities, the data has been detrended (see section 3) and the component of the variance linearly associated with the QBO at 50hPa two months prior has been removed. Winters categorized as Central Pacific ENSO are in black, Eastern Pacific ENSO are in blue, and all other years in red. A linear least-squares best fit is shown in each panel, and the slope is indicated.

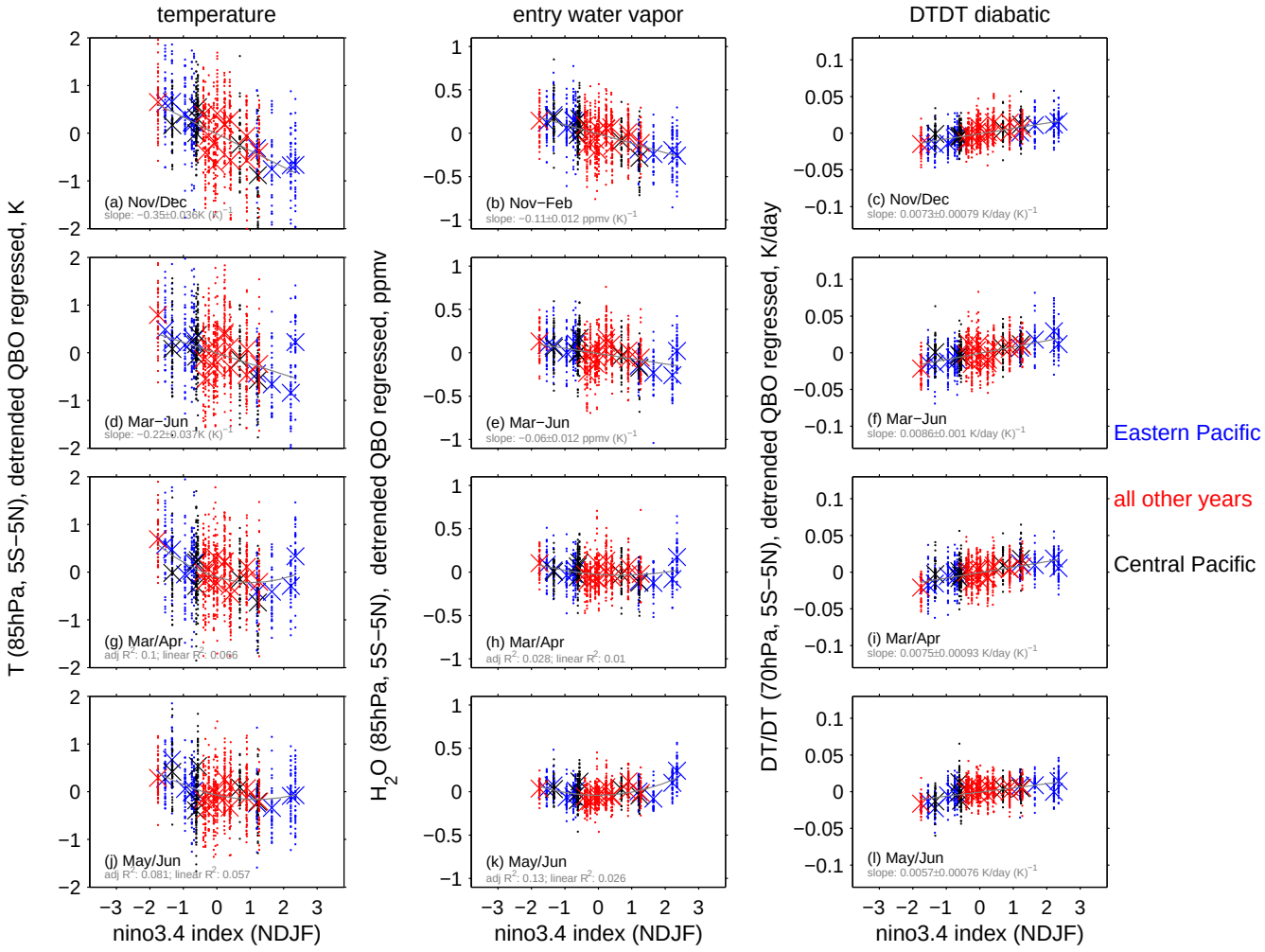

Figure 3. As in Figure 2 but for 42 AGCM GEOSCCM integrations. The ensemble mean response is indicated with a large x, and each integration with a dot.

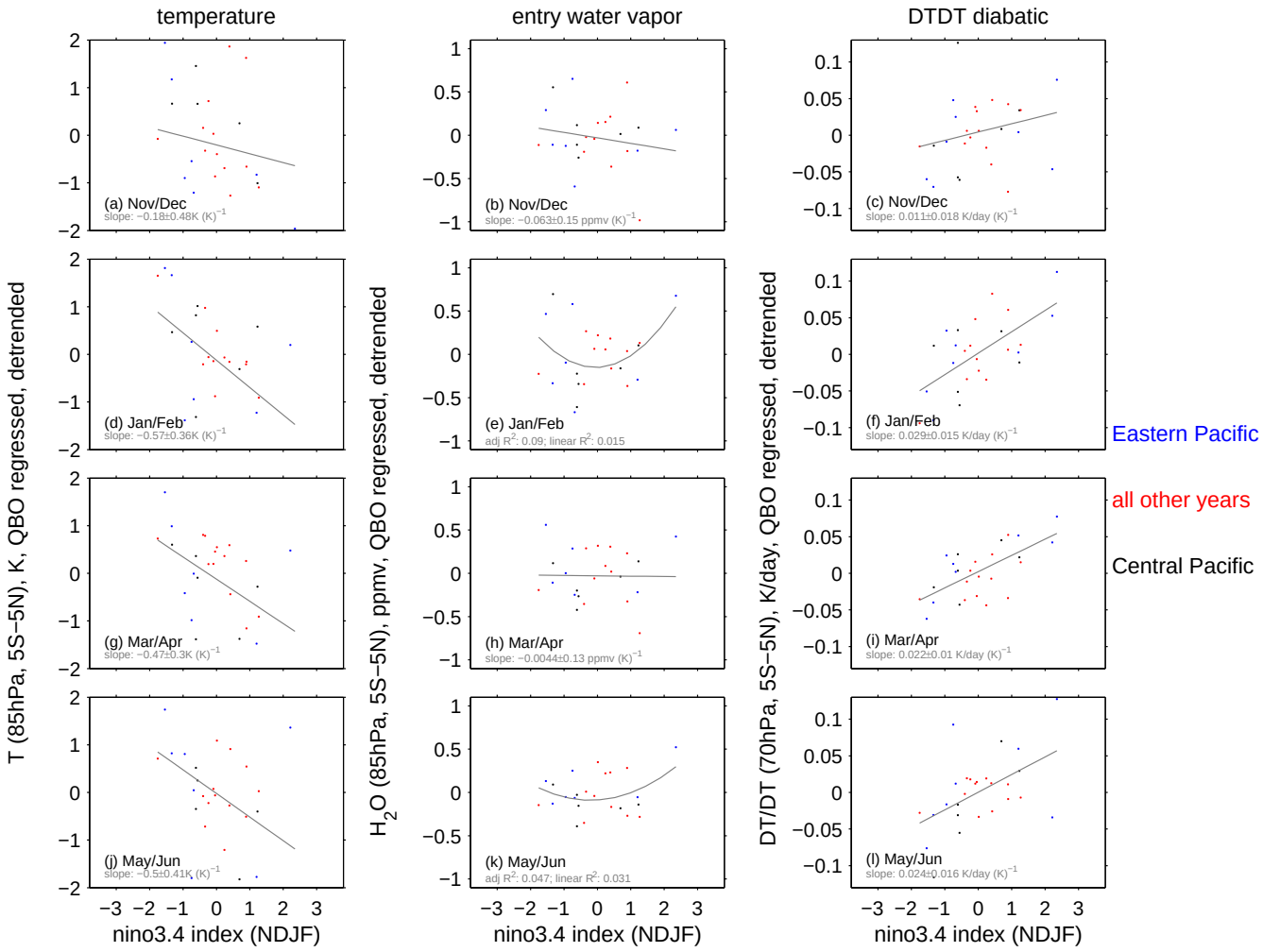

Figure 4. As in Figure 2 and 3 but for the MERRA reanalysis (left and right columns) and SWOOSH (middle column).

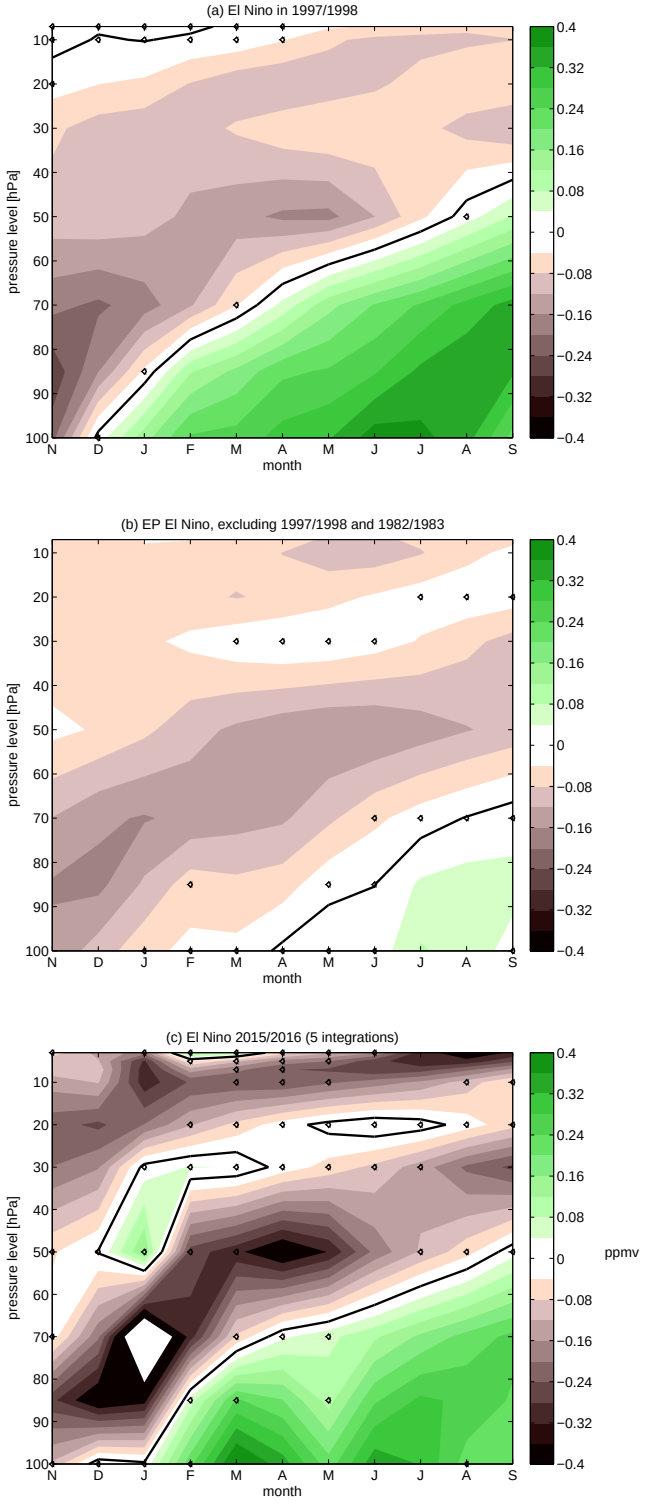

Figure 5. Water vapor anomalies (ppmv) for the 42 GEOSCCM integrations in (a) 97/98; (b) all EPEN events except 97/98 and 82/83; (c) 2015/2016 in the 5 experiments that have been extended to the near present. Anomalies that are not significant at the 95% level are marked by black symbols. The effect of the QBO at 50hPa and the linear trend have been linearly regressed out of all anomalies.

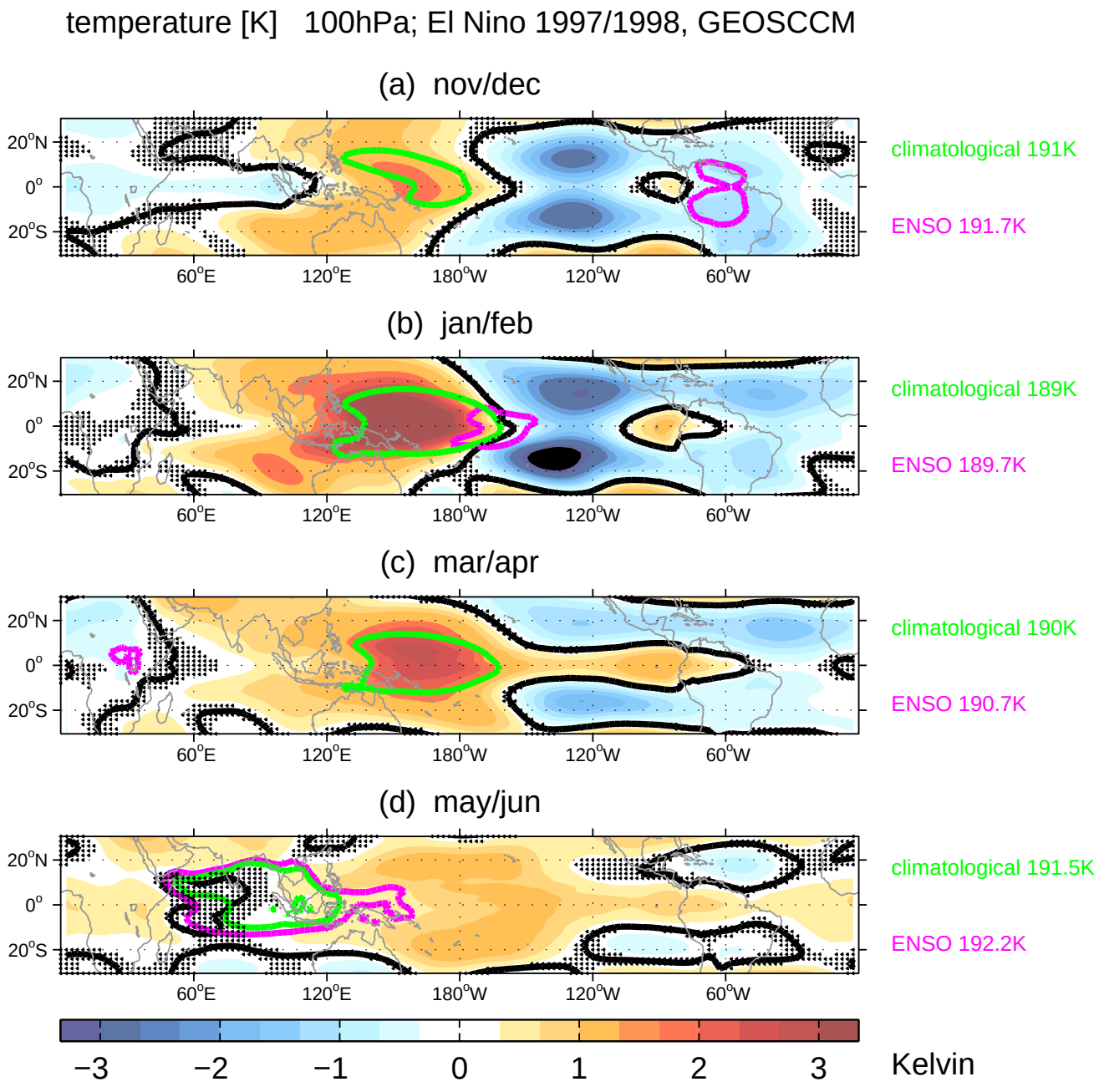

Figure 6. Temperature anomalies (Kelvin) at 100hPa for 1997/1998 in the GEOSCCM AGCM integrations in November/December (top) through the following May/June (bottom). Anomalies that are not significant at the 95% level are marked by black symbols. The green and magenta contours denote specific cold isotherms in the climatology and for this specific composite in order to highlight the location of the cold point. The effect of the QBO at 50hPa and the linear trend have been linearly regressed out of all anomalies. The contour interval is 1/3K.

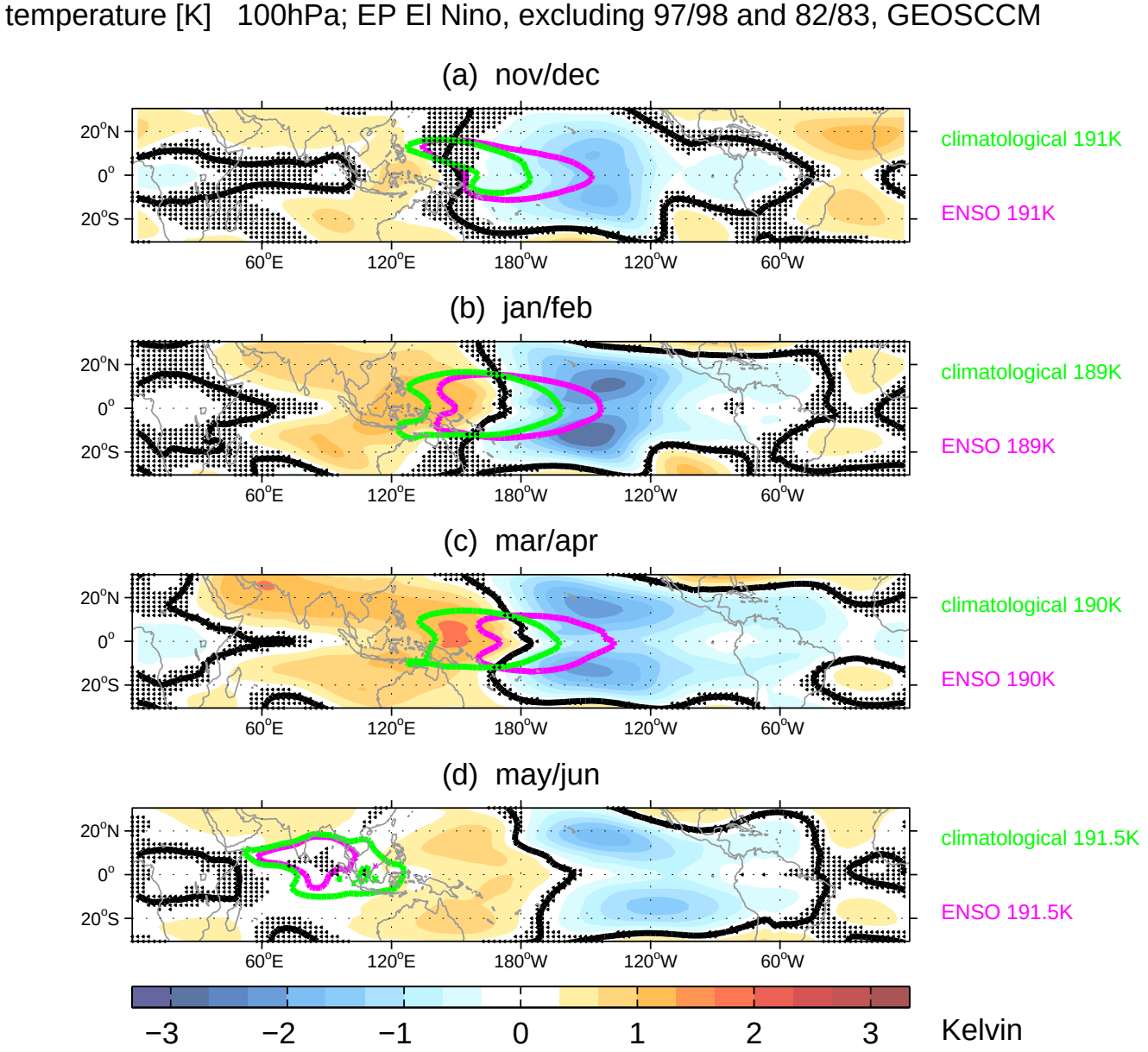

Figure 7. As in figure 6 but for all ENSO events except 1982/1983 and 1997/1998 in the GEOSCCM AGCM integrations.

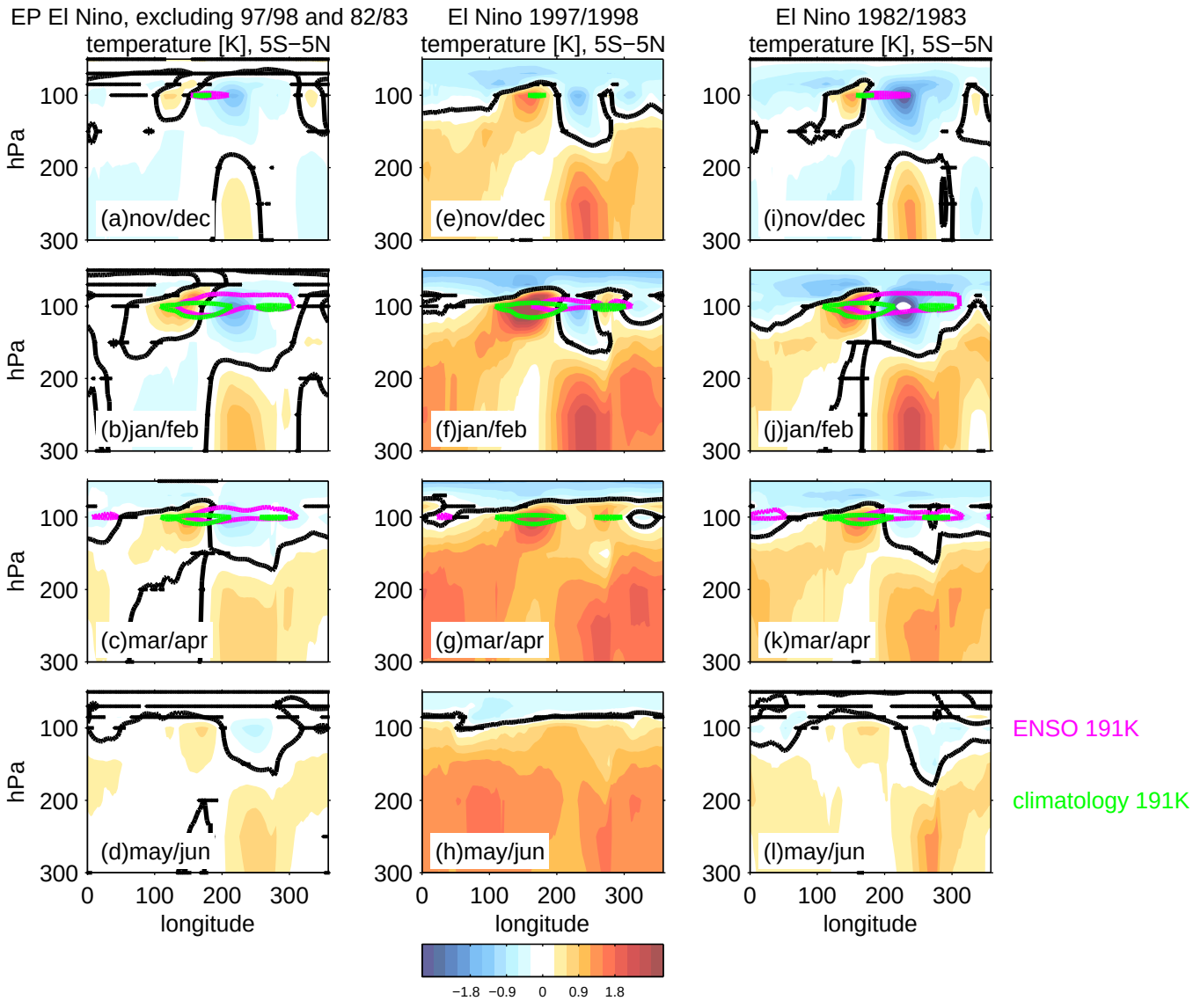

Figure 8. Tropical (5S-5N) temperature anomalies (Kelvin) for (a-d)for all EP EN events excluding 97/98 and 82/83, (e-h) 97/98, and (i-l) 82/83, in the AGCM simulations. Anomalies that are not significant at the 95% level are marked by black symbols. The green and magenta contours denote specific cold isotherms in the climatology and for this specific composite in order to highlight the location of the cold point. The effect of the QBO at 50hPa and the linear trend have been linearly regressed out of all anomalies. The contour interval is 0.3K.

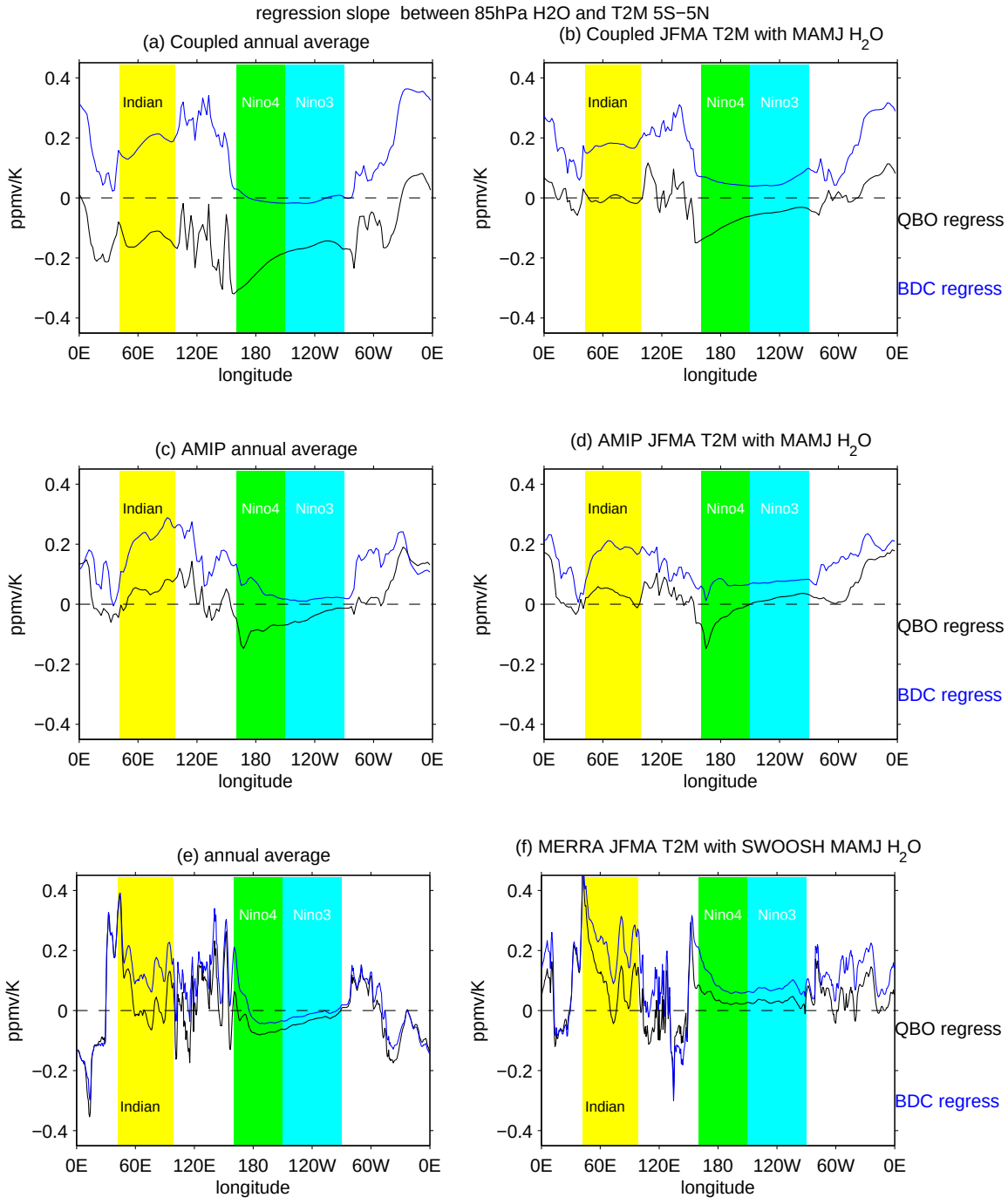

Figure 9. Regression coefficent between tropical (5S-5N) T2m and zonally averaged entry water vapor at 85hPa in (a-b) the last 240 years of a coupled ocean-atmosphere run; (c-d) the AMIP runs; (e-f) for SWOOSH water varpor and MERRA 2 meter temperatures. The longitude bands corresponding to the Indian Ocean, Nino3, and Nino4 regions are in color. The left column is for annual averaged quantities and the right column is for springtime (March through June) water vapor with T2m two months prior.

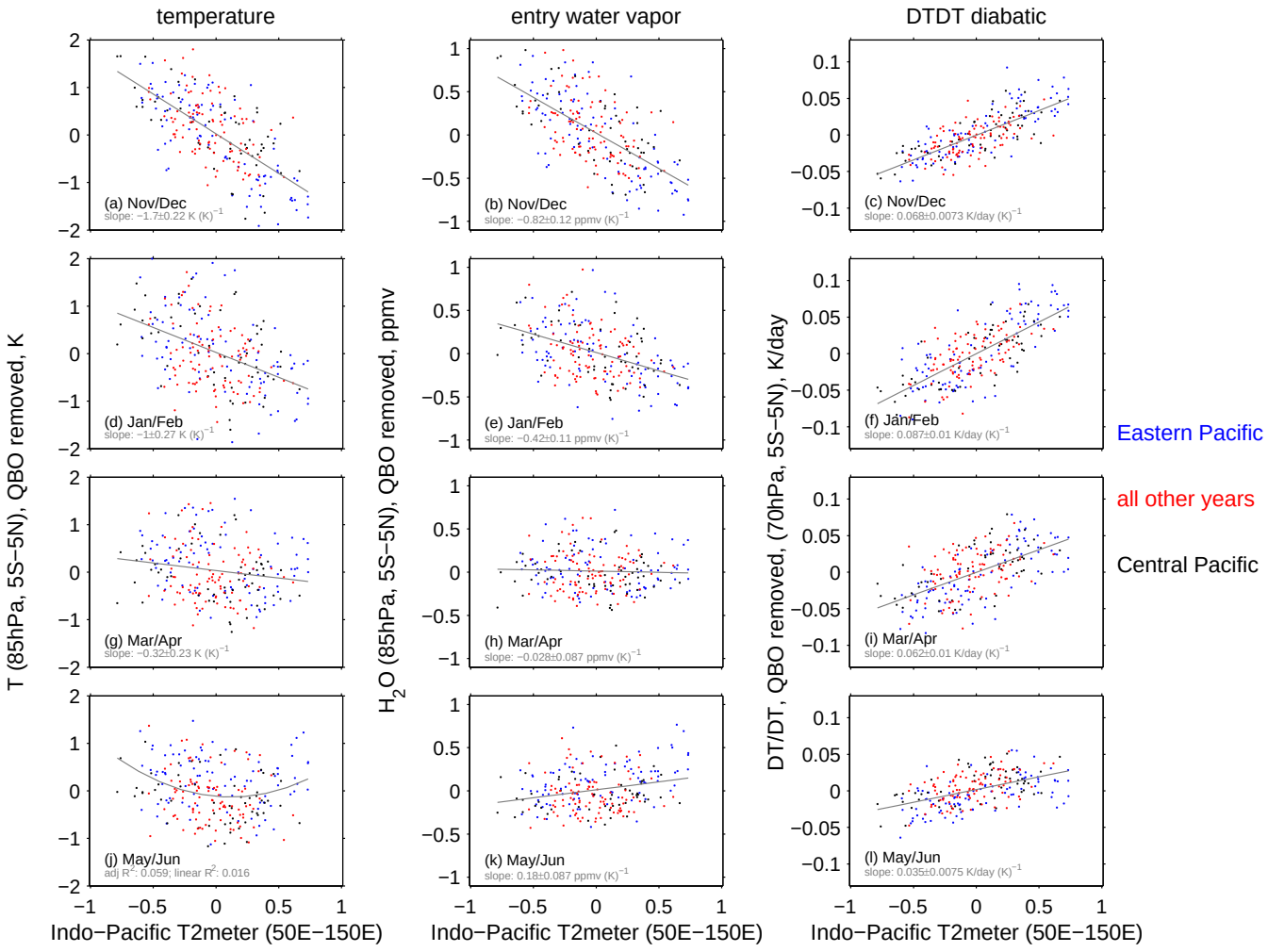

Figure 10. As in Figure 2 but stratifying years based on 2meter temperature from 50E to 150E, 5S-5N.

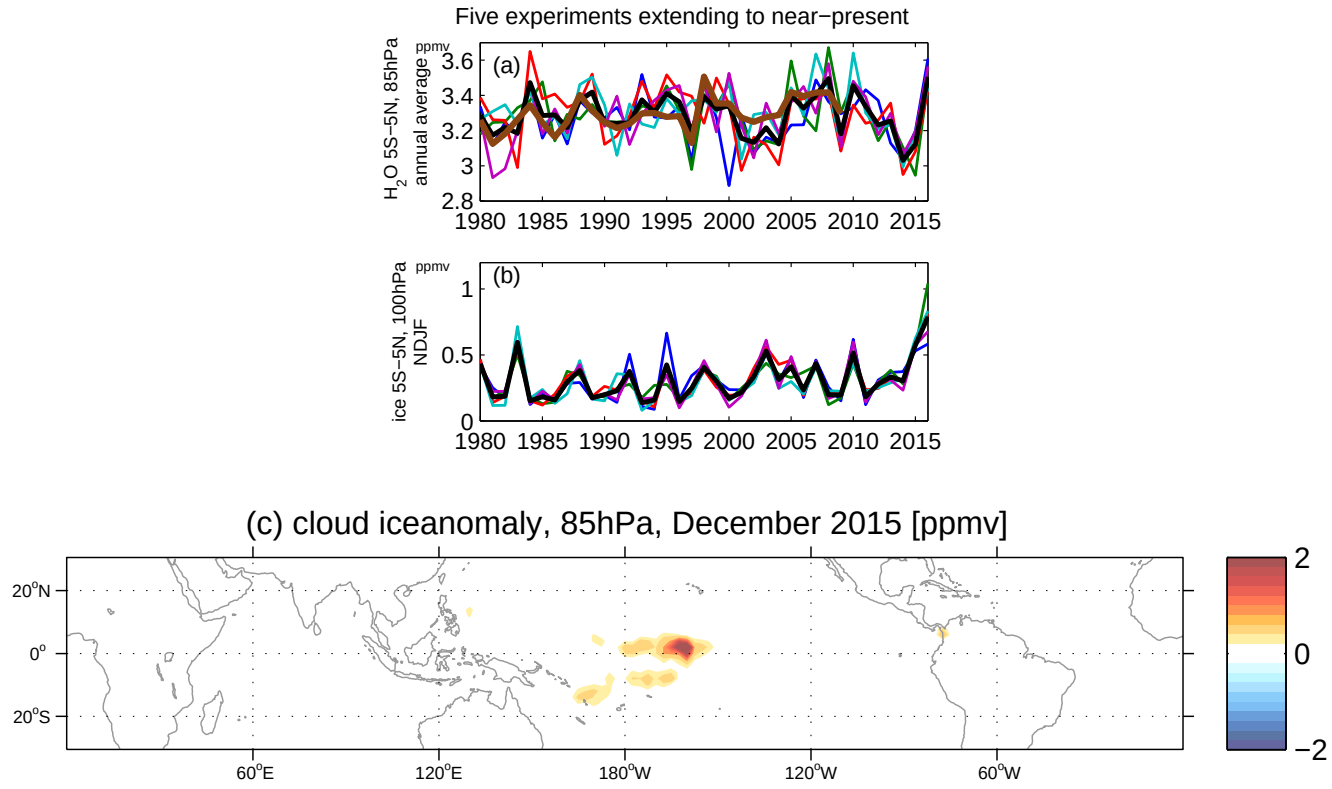

Figure 11. Annual average water anomalies at 85hPa for the GEOSCCM AGCM experiments. (a) 85hPa water vapor between 5S and 5N. (b) Cloud ice at 100hPa between 5S and 5N. The thick brown line in (a) indicates the averaged across all 42 AMIP integrations. A black line indicates the ensemble mean of the five integrations which have been extended to the near-present, and color indicates each of these five simulations. (c) Cloud ice anomalies at 85hPa in December 2015 in the ensemble mean of these five simulations. No detrending has been performed on any of the timeseries.

Acknowledgements. CIG was supported by the Israel Science Foundation (grant number 1558/14) and by a European Research Council starting grant under the European Union's Horizon 2020 research and innovation programme (grant agreement No 677756). We thank those involved in model development at GSFC-GMAO, and support by the NASA MAP program. We thank Valentina Aquila for performing some of the experiments discussed here, and Darryn W Waugh and Margaret M Hurwitz for suggestions. High-performance computing resources were provided by the NASA Center for Climate Simulation (NCCS). Correspondence and requests for data should be addressed to C.I.G. (email: chaim.garfinkel@mail.huji.ac.il). El Niño indices based on the ERSSTv4 data were downloaded from cpc.ncep.noaa.gov/data/indices/ersst4.nino.mth.81-10.ascii.

References

Aquila, V., Swartz, W. H., Colarco, P. R., Pawson, S., Polvani, L. M., Stolarski, R. S., and Waugh, D. W.: Attributing changes in global stratospheric temperatures using model integrations with incrementally added single forcings, Journal of Geophysical Research: Atmospheres, in press, doi:10.1002/2015JD023841, 2016.

Avery, M. A., Davis, S. M., Rosenlof, K. H., Ye, H., and Dessler, A.: Large anomalies in lower stratospheric water vapor and ice during the 2015-2016 El Nino, Nature Geosciences, 10, doi:10.1038/ngeo2961, 2017.

Bonazzola, M. and Haynes, P.: A trajectory-based study of the tropical tropopause region, Journal of Geophysical Research: Atmospheres, 109, doi:10.1029/2003JD004356, 2004.

Brinkop, S., Dameris, M., Jöckel, P., Garny, H., Lossow, S., and Stiller, G.: The millennium water vapour drop in chemistry–climate model simulations, Atmospheric Chemistry and Physics, 16, 8125–8140, 2016.

Calvo, N., Garcia, R., Randel, W., and Marsh, D.: Dynamical mechanism for the increase in tropical upwelling in the lowermost tropical stratosphere during warm ENSO events, Journal of the Atmospheric Sciences, 67, 2331–2340, 2010.

Calvo Fernández, N., García, R. R., García Herrera, R., Gallego Puyol, D., Gimeno Presa, L., Hernández Martín, E., and Ribera Rodríguez, P.: Analysis of the ENSO Signal in Tropospheric and Stratospheric Temperatures Observed by MSU, 1979 2000., Journal of Climate, 17, 3934–3946, doi:10.1175/1520-0442(2004)017<3934:AOTESI>2.0.CO;2, 2004.

Chatterjee, S. and Hadi, A. S.: Regression analysis by example-fifth edition, John Wiley & Sons, 2012.

Crooks, S. A. and Gray, L. J.: Characterization of the 11-Year Solar Signal Using a Multiple Regression Analysis of the ERA-40 Dataset, J. Clim., 18, 996–1015, 2005.

Davis, S. M., Liang, C. K., and Rosenlof, K. H.: Interannual variability of tropical tropopause layer clouds, Geophysical Research Letters, 40, 2862–2866, 2013.

Davis, S. M., Rosenlof, K. H., Hassler, B., Hurst, D. F., Read, W. G., Vömel, H., Selkirk, H., Fujiwara, M., and Damadeo, R.: The Stratospheric Water and Ozone Satellite Homogenized (SWOOSH) database: A long-term database for climate studies, Earth System Science Data, 8, 461, 2016.

Dessler, A., Schoeberl, M., Wang, T., Davis, S., and Rosenlof, K.: Stratospheric water vapor feedback, Proceedings of the National Academy of Sciences, 110, 18 087–18 091, 2013.

Dessler, A., Schoeberl, M., Wang, T., Davis, S., Rosenlof, K., and Vernier, J.-P.: Variations of stratospheric water vapor over the past three decades, Journal of Geophysical Research: Atmospheres, 119, doi:10.1002/2014JD021712, 2014.

Fletcher, C. and Kushner, P.: The role of linear interference in the Annular Mode response to Tropical SST forcing, J. Clim., 24, 778–794, doi:10.1175/2010JCLI3735.1, 2011.

Forster, P. M. and Shine, K. P.: Stratospheric water vapor changes as a possible contributor to observed stratospheric cooling, Geophys. Res. Lett., 26, 3309–3312, doi:10.1029/1999GL010487, 1999.

Free, M. and Seidel, D. J.: Observed El Niño-Southern Oscillation temperature signal in the stratosphere, J. Geophys. Res., 114, D23108, doi:10.1029/2009JD012420, 2009.

Fueglistaler, S.: Stepwise changes in stratospheric water vapor?, Journal of Geophysical Research (Atmospheres), 117, D13302, doi:10.1029/2012JD017582, 2012.

Fueglistaler, S. and Haynes, P.: Control of interannual and longer-term variability of stratospheric water vapor, Journal of geophysical research, 110, D24 108, 2005.

Fueglistaler, S., Wernli, H., and Peter, T.: Tropical troposphere-to-stratosphere transport inferred from trajectory calculations, Journal of Geophysical Research (Atmospheres), 109, D03108, doi:10.1029/2003JD004069, 2004.

Fueglistaler, S., Liu, Y., Flannaghan, T., Haynes, P., Dee, D., Read, W., Remsberg, E., Thomason, L., Hurst, D., Lanzante, J., et al.: The relation between atmospheric humidity and temperature trends for stratospheric water, Journal of Geophysical Research: Atmospheres, 2013.

Fueglistaler, S., Abalos, M., Flannaghan, T., Lin, P., and Randel, W.: Variability and trends in dynamical forcing of tropical lower stratospheric temperatures, Atmospheric Chemistry and Physics, 14, 13 439–13 453, doi:10.5194/acp-14-13439-2014, 2014.

Garcia-Herrera, R., Calvo, N., Garcia, R. R., and Giorgetta, M. A.: Propagation of ENSO Temperature Signals into the Middle Atmosphere: A Comparison of Two General Circulation Models and ERA-40 Reanalysis Data, J. Geophys. Res., D06101, doi:10.1029/2005JD006061, 2006.

Garfinkel, C. I. and Hartmann, D. L.: Effects of the El-Nino Southern Oscillation and the Quasi-Biennial Oscillation on polar temperatures in the stratosphere, J. Geophys. Res.- Atmos., 112, D19112, doi:10.1029/2007JD008481, 2007.

Garfinkel, C. I. and Hartmann, D. L.: Different ENSO Teleconnections and Their Effects on the Stratospheric Polar Vortex, J. Geophys. Res.-Atmos., 113, doi:10.1029/2008JD009920, 2008.

Garfinkel, C. I., Hurwitz, M., Oman, L., and Waugh, D. W.: Contrasting Effects of Central Pacific and Eastern Pacific El Nino on Stratospheric Water Vapor, Geophys. Res. Lett., in press, 2013a.

Garfinkel, C. I., Waugh, D. W., Oman, L., Wang, L., and Hurwitz, M.: Upper tropospheric and lower stratospheric zonally asymmetric tropical temperature trends forced by sea surface temperature trends: implications for water vapor and ozone, J. Geophys. Res.- Atmos., 118, 9658–9672, doi:10.1002/jgrd.50772, 2013b.

Garfinkel, C. I., Waugh, D. W., and Polvani, L. M.: Recent Hadley cell expansion: The role of internal atmospheric variability in reconciling modeled and observed trends, Geophysical Research Letters, 42, 2015.

Garfinkel, C. I., Aquila, V., Waugh, D. W., and Oman, L. D.: Time-varying changes in the simulated structure of the Brewer–Dobson Circulation, Atmospheric Chemistry and Physics, 17, 1313–1327, 2017.

Gettelman, A., Randel, W., Massie, S., Wu, F., Read, W., and Russell III, J.: El Nino as a natural experiment for studying the tropical tropopause region, Journal of climate, 14, 3375–3392, 2001.

Gilford, D. M., Solomon, S., and Portmann, R. W.: Radiative impacts of the 2011 abrupt drops in water vapor and ozone in the tropical tropopause layer, Journal of Climate, 29, 595–612, 2016.

Griffies, S. M., Winton, M., Anderson, W. G., Benson, R., Delworth, T. L., Dufour, C. O., Dunne, J. P., Goddard, P., Morrison, A. K., Rosati, A., et al.: Impacts on ocean heat from transient mesoscale eddies in a hierarchy of climate models, Journal of Climate, 28, 952–977, 2015.

Hasebe, F. and Noguchi, T.: A Lagrangian description on the troposphere-to-stratosphere transport changes associated with the stratospheric water drop around the year 2000, Atmospheric Chemistry and Physics, 16, 4235–4249, doi:10.5194/acp-16-4235-2016, 2016.

Huang, B., Banzon, V. F., Freeman, E., Lawrimore, J., Liu, W., Peterson, T. C., Smith, T. M., Thorne, P. W., Woodruff, S. D., and Zhang, H.-M.: Extended reconstructed sea surface temperature version 4 (ERSST. v4). Part I: Upgrades and intercomparisons, Journal of climate, 28, 911–930, 2015.

Hurwitz, M. M., Calvo, N., Garfinkel, C. I., Butler, A. H., Ineson, S., Cagnazzo, C., Manzini, E., and Peña-Ortiz, C.: Extra-tropical atmospheric response to ENSO in the CMIP5 models, Climate dynamics, 43, 3367–3376, 2014.

Johnson, N. C.: How many ENSO flavors can we distinguish?, Journal of Climate, 26, 4816–4827, 2013.

Konopka, P., Ploeger, F., Tao, M., and Riese, M.: Zonally resolved impact of ENSO on the stratospheric circulation and water vapor entry values, Journal of Geophysical Research: Atmospheres, 121, 2016.

Li, F., Vikhliaev, Y. V., Newman, P. A., Pawson, S., Perlwitz, J., Waugh, D. W., and Douglass, A. R.: Impacts of Interactive Stratospheric Chemistry on Antarctic and Southern Ocean Climate Change in the Goddard Earth Observing System, Version 5 (GEOS-5), Journal of Climate, 29, 3199–3218, 2016.

Liang, C., Eldering, A., Gettelman, A., Tian, B., Wong, S., Fetzer, E., and Liou, K.: Record of tropical interannual variability of temperature and water vapor from a combined AIRS-MLS data set, Journal of Geophysical Research, 116, D06 103, 2011.

Manzini, E., Giorgetta, M. A., Kornbluth, L., and Roeckner, E.: The Influence of Sea Surface Temperatures on the Northern Winter Stratosphere: Ensemble Simulations with the MAECHAM5 Model, J. Clim., 19, 3863–3881, 2006.

Marsh, D. R. and Garcia, R. R.: Attribution of decadal variability in lower-stratospheric tropical ozone, Geophysical Research Letters, 34, 2007.

Meinshausen, M., Smith, S. J., Calvin, K., Daniel, J. S., Kainuma, M., Lamarque, J., Matsumoto, K., Montzka, S., Raper, S., Riahi, K., et al.: The RCP greenhouse gas concentrations and their extensions from 1765 to 2300, Climatic change, 109, 213–241, 2011.

Mitchell, D., Gray, L., Fujiwara, M., Hibino, T., Anstey, J., Ebisuzaki, W., Harada, Y., Long, C., Misios, S., Stott, P., et al.: Signatures of naturally induced variability in the atmosphere using multiple reanalysis datasets, Quarterly Journal of the Royal Meteorological Society, doi:10.1002/qj.2492, 2015.

Molod, A., Takacs, L., Suarez, M., Bacmeister, J., Song, I.-S., and Eichmann, A.: The GEOS-5 Atmospheric General Circulation Model: Mean Climate and Development from MERRA to Fortuna, Technical Report Series on Global Modeling and Data Assimilation, 28, https://gmao.gsfc.nasa.gov/pubs/docs/Molod484.pdf, 2012.

Moorthi, S. and Suarez, M. J.: Relaxed Arakawa-Schubert. A Parameterization of Moist Convection for General Circulation Models, Monthly Weather Review, 120, 978, doi:10.1175/1520-0493(1992)120<0978:RASAPO>2.0.CO;2, 1992.

Mote, P. W., Rosenlof, K. H., McIntyre, M. E., Carr, E. S., Gille, J. C., Holton, J. R., Kinnersley, J. S., Pumphrey, H. C., Russell, III, J. M., and Waters, J. W.: An atmospheric tape recorder: The imprint of tropical tropopause temperatures on stratospheric water vapor, J. Geophys. Res., 101, 3989–4006, doi:10.1029/95JD03422, 1996.

Murtugudde, R., McCreary, J. P., and Busalacchi, A. J.: Oceanic processes associated with anomalous events in the Indian Ocean with relevance to 1997–1998, Journal of Geophysical Research: Oceans, 105, 3295–3306, 2000.

Oman, L., Waugh, D. W., Pawson, S., Stolarski, R. S., and Nielsen, J. E.: Understanding the Changes of Stratospheric Water Vapor in Coupled Chemistry-Climate Model Simulations, Journal of Atmospheric Sciences, 65, 3278, doi:10.1175/2008JAS2696.1, 2008.

Pawson, S., Stolarski, R. S., Douglass, A. R., Newman, P. A., Nielsen, J. E., Frith, S. M., and Gupta, M. L.: Goddard Earth Observing System chemistry-climate model simulations of stratospheric ozone-temperature coupling between 1950 and 2005, Journal of Geophysical Research (Atmospheres), 113, D12103, doi:10.1029/2007JD009511, 2008.

Randel, W. J., Wu, F., and Gaffen, D. J.: Interannual variability of the tropical tropopause derived from radiosonde data and NCEP reanalyses, Journal of Geophysical Research, 105, 15–509, 2000.

Randel, W. J., Wu, F., Oltmans, S. J., Rosenlof, K., and Nedoluha, G. E.: Interannual changes of stratospheric water vapor and correlations with tropical tropopause temperatures, Journal of the Atmospheric Sciences, 61, 2133–2148, 2004.

Randel, W. J., Wu, F., Vömel, H., Nedoluha, G. E., and Forster, P.: Decreases in Stratospheric Water Vapor after 2001: Links to Changes in the Tropical Tropopause and the Brewer-Dobson Circulation, J. Geophys. Res., 111, D12312, 2006.

Rayner, N., Brohan, P., Parker, D., Folland, C., Kennedy, J., Vanicek, M., Ansell, T., and Tett, S.: Improved analyses of changes and uncertainties in sea surface temperature measured in situ since the mid-nineteenth century: The HadSST2 dataset, Journal of Climate, 19, 446–469, doi:10.1175/JCLI3637.1, 2006.

Reynolds, R. W., Rayner, N. A., Smith, T. M., Stokes, D. C., and Wang, W.: An improved in situ and satellite SST analysis for climate, Journal of climate, 15, 1609–1625, doi:10.1175/1520-0442(2002)015<1609:AIISAS>2.0.CO;2, 2002.

Rienecker, M. M., Suarez, M. J., Gelaro, R., Todling, R., Bacmeister, J., Liu, E., Bosilovich, M. G., Schubert, S. D., Takacs, L., Kim, G.-K., Bloom, S., Chen, J., Collins, D., Conaty, A., da Silva, A., Gu, W., Joiner, J., Koster, R. D., Lucchesi, R., Molod, A., Owens, T., Pawson, S., Pegion, P., Redder, C. R., Reichle, R., Robertson, F. R., Ruddick, A. G., Sienkiewicz, M., and Woollen, J.: MERRA: NASA's Modern-Era Retrospective Analysis for Research and Applications, Journal of Climate, 24, 3624–3648, doi:10.1175/JCLI-D-11-00015.1, 2011.

Rienecker et al, M. M.: The GEOS-5 Data Assimilation System - Documentation of Versions 5.0.1, 5.1.0, and 5.2.0, Technical Report Series on Global Modeling and Data Assimilation, 27, http://gmao.gsfc.nasa.gov/pubs/docs/Rienecker369.pdf, 2008.

Rosenlof, K. H. and Reid, G. C.: Trends in the temperature and water vapor content of the tropical lower stratosphere: Sea surface connection, Journal of Geophysical Research (Atmospheres), 113, D06107, doi:10.1029/2007JD009109, 2008.

Sassi, F., Kinnison, D., Bolville, B. A., Garcia, R. R., and Roble, R.: Effect of El-Niño Southern Oscillation on the Dynamical, Thermal, and Chemical Structure of the Middle Atmosphere, J. Geophys. Res., D17108, doi:10.1029/2003JD004434, 2004.

Scherllin-Pirscher, B., Deser, C., Ho, S.-P., Chou, C., Randel, W., and Kuo, Y.-H.: The vertical and spatial structure of ENSO in the upper troposphere and lower stratosphere from GPS radio occultation measurements, Geophysical Research Letters, 39, n/a–n/a, doi:10.1029/2012GL053071, http://dx.doi.org/10.1029/2012GL053071, 2012.

Schott, F. A., Xie, S.-P., and McCreary, J. P.: Indian Ocean circulation and climate variability, Reviews of Geophysics, 47, doi:10.1029/2007RG000245, 2009.

Simpson, I. R., Shepherd, T. G., and Sigmond, M.: Dynamics of the lower stratospheric circulation response to ENSO, Journal of the Atmospheric Sciences, 68, 2537–2556, 2011.

Solomon, S., Garcia, R. R., Rowland, F. S., and Wuebbles, D. J.: On the depletion of Antarctic ozone, nature, 321, 755–758, doi:10.1038/321755a0, 1986.

Solomon, S., Rosenlof, K. H., Portmann, R. W., Daniel, J. S., Davis, S. M., Sanford, T. J., and Plattner, G.-K.: Contributions of Stratospheric Water Vapor to Decadal Changes in the Rate of Global Warming, Science, 327, 1219–, doi:10.1126/science.1182488, 2010.

SPARC-CCMVal: SPARC Report on the Evaluation of Chemistry-Climate Models, SPARC Report, 5, WCRP-132, WMO/TD-No. 1526, http://www.sparc-climate.org/publications/sparc-reports/sparc-report-no5/, 2010.

Su, H., Neelin, J. D., and Chou, C.: Tropical teleconnection and local response to SST anomalies during the 1997–1998 El Nino, Journal of Geophysical Research: Atmospheres, 106, 20 025–20 043, 2001.

Taguchi, M. and Hartmann, D. L.: Increased Occurrence of Stratospheric Sudden Warming During El Niño as Simulated by WAACM, J. Clim., 19, 324–332, doi:10.1175/JCLI3655.1, 2006.

Urban, J., Lossow, S., Stiller, G., and Read, W.: Another drop in water vapor, Eos, Transactions American Geophysical Union, 95, 245–246, 2014.

Webster, P. J., Moore, A. M., Loschnigg, J. P., and Leben, R. R.: Coupled ocean-atmosphere dynamics in the Indian Ocean during 1997-98, Nature, 401, 356, 1999.

World Meteorological Organization: Scientific Assessment of Ozone Depletion: 2010, Global Ozone Research and Monitoring Project Rep. No. 52, 2011.

World Meteorological Organization: Scientific Assessment of Ozone Depletion: 2014, Global Ozone Research and Monitoring Project Rep. No. 55, 2014.

Xie, S.-P., Hu, K., Hafner, J., Tokinaga, H., Du, Y., Huang, G., and Sampe, T.: Indian Ocean capacitor effect on Indo–western Pacific climate during the summer following El Niño, Journal of Climate, 22, 730–747, doi:10.1175/2008JCLI2544.1, 2009.

Yu, L. and Rienecker, M. M.: Indian Ocean warming of 1997–1998, Journal of Geophysical Research: Oceans, 105, 16 923–16 939, 2000.

Yulaeva, E. and Wallace, J. M.: The signature of ENSO in global temperature and precipitation fields derived from the microwave sounding unit, Journal of climate, 7, 1719–1736, 1994.

Zhou, X. L., Geller, M. A., and Zhang, M. H.: Tropical cold point tropopause characteristics derived from ECMWF reanalyses and soundings, Journal of climate, 14, 1823–1838, 2001.